Engineering Fracture Mechanics 76 (2009) 439–453

Contents lists available at ScienceDirect

Engineering Fracture Mechanics

journal homepage: www.elsevier.com/locate/engfracmech

Elastic notch stress intensity factors for sharply V-notched rounded bars under torsion

M. Zappalorto, P. Lazzarin *, F. Berto

Department of Management and Engineering, University of Padova, Stradella San Nicola 3, 36100 Vicenza, Italy

ARTICLE INFO

Article history:
Received 18 July 2008
Received in revised form 4 November 2008
Accepted 26 November 2008
Available online 3 December 2008

Keywords:
Elastic stress distributions
Notch stress intensity factors (NSIFs)
Torsion

ABSTRACT

The paper deals with the determination of analytical expressions for the mode III notch stress intensity factors for circumferentially-sharply-notched rounded bars under torsion loading, starting from the theoretical stress concentration factors of the corresponding notch problem.

An exact, closed-form solution for the NSIFs is obtained for deep notches; subsequently the solution is extended also to finite notched components taking advantage of a shape function determined by a numerical best fitting procedure.

1. Introduction

While the linear elastic stress fields in the vicinity of the crack tip were first determined by Westergaard [1], the asymptotic nature of the stress fields due to pointed V-notches was first documented by Williams [2] who demonstrated that the degree of singularity of mode I and mode II stress distributions depends on the V-notch angle. The intensity of the stress field was later given in terms of notch (or generalised) stress intensity factors, NSIFs, by Gross and Mendelson [3] who also provided a set of NSIFs from V-notches in plates. Subsequently the stress distributions due to sharp V-notches under antiplane shear were given by Seweryn and Molski [4], Dunn et al. [5], and Qian and Hasebe [6].

In the context of a stress field theory, the NSIFs were applied to the fracture toughness of components made of brittle materials (see among the others, Nui et al. [7], Dunn et al. [8,9], Gomez and Elices [10,11]) as well as for fatigue crack initiation assessments at notches and weld toes (Boukharouba et al. [12], Verreman and Nie [13]). Gomez and Elices [11] were able to demonstrate that a single non-dimensional curve provides an accurate fit of experimental data from static tests carried out on V-notched specimens of steel, aluminum, PMMA and PVC. Their master curve plots as a function of the notch angle a non-dimensional parameter which combines together the critical value of the NSIF, the fracture toughness K_{IC} and a characteristic length of the material L_{ch}. Good agreement between computed and measured failure loads were obtained by Gomez and Elices not only for ideally sharp notches and brittle fracture, but also when root radii were small (typically less than 0.05 mm) and when plasticity was contained. Dealing with fatigue problems it was noted by Verreman and Nie [13] that for engineering applications it is too complex to take into account the non-LEFM behaviour of a short crack and the multiple crack interaction on different planes influenced by loading parameters and statistical variations related to the irregularity of the toe profile. In these works it was assumed that a crack propagates from the notch tip when the actual value of the NSIF reaches a critical value. Under favourable circumstances, not only the fatigue crack initiation life but also the total fatigue life can be controlled by the NSIFs (Lazzarin and Tovo [14], Atzori et al. [15], Lazzarin and Livieri [16]). This occurs

* Corresponding author.
E-mail address: plazzarin@gest.unipd.it (P. Lazzarin).

0013-7944/$ - see front matter © 2008 Elsevier Ltd. All rights reserved.
doi:10.1016/j.engfracmech.2008.11.008

Nomenclature

a	notch depth
R	radius of the net section for the solid round bar
R_n	external radius of the net section for the hollow round bar
R_i	internal radius of the net section for the hollow round bar
R_g	radius of the Gross section for the round bar
ρ	notch root radius
2α	V-notch opening angle
q	parameter linked to the V-notch opening angle 2α
r_0	distance between the notch tip and the origin of the polar coordinate system
r, φ	polar coordinates
u, v	curvilinear coordinates in Neuber's auxiliary system
λ_3	linear elastic eigenvalue for mode III V-notch stress distribution
K	r_0/R
κ_1	r_0/R_n
κ_2	R_i/R_n
ψ	R/a
s_3	$\lambda_3 - 1$
τ_n	nominal shear stress on the net sectional area
τ_{xz}, τ_{yz}	shear stress components in the cartesian coordinate system
τ_{max}	maximum notch stress
K_I	stress intensity factor under mode I (crack case)
$K_{3,\rho}$	notch stress intensity factor for the mode III loaded rounded notch
K_{tn}	theoretical stress concentration factor referred to the net section
K_{III}	stress intensity factor under mode III (crack case)
K_3^V	notch stress intensity factor (NSIF) for mode III stress distribution
$\bar{K}_3^V$	NSIF normalised with respect to the nominal shear stress on the net sectional area
k_{3d}	non-dimensional shape factor for the deep sharp V-notch
k_{3h}	non-dimensional shape factor for the deep sharp V-notch in a hollow round bar
k_{3s}	non-dimensional shape factor for the shallow sharp V-notch
k_3	non-dimensional shape factor for the sharp V-notch of finite size
F_{IIIs}	$k_{3s}/\sqrt{\pi}$
F_{III}	shape function of the notch of arbitrary depth
η	F_{III}/F_{IIIs}
Δ	relative deviation
f_{B-K}	shape function in Benthem and Koiter's solution

when a large amount of the fatigue life of welded samples is consumed at short crack depth, within the zone governed by the V-notch singularity. No demarcation line being drawn between fatigue crack initiation and early propagation, both phases were thought of as strictly dependent on the stress distribution of the uncracked component, that is from the NSIFs.

When the singularity degree is constant the NSIFs can be compared directly, without any assumption regarding the actual entity that drives the failure phenomenon. Reedy [17] and Reedy and Guess [18], for example, correlated failure of adhesive-bonded butt tensile joints with a generalized stress intensity at the free edge of the interface between elastic and rigid layers. The degree of singularity in those specimens was −0.33; the same value was found to characterise the weld toe region when the V-notch angle is 135° [14].

On parallel tracks, great efforts have been done to derive closed-form solutions for the stress intensity factors (SIFs) for a number of simple configurations starting from the analytical expressions of the stress fields. The analytical approach typically needs some mathematical abstractions, such as the presence of cracks in a body of infinite size. For a major number of cases of engineering interest in terms of configuration and boundary conditions, accurate values of the SIFs are obtained numerically by using the Weight Function method, the Mapping Collocation Technique, the Body Force method and so on (Aliabadi et al. [19], Anderson [20]) and are collected in some well known handbooks (Tada, Paris and Irwin [21], Murakami [22]). The idea of estimating the theoretical stress concentration factor from the Stress Intensity Factor of an equivalent crack has also been discussed in the literature (Shin et al. [23] and Livieri [24]), at least for geometries where the influence of the notch opening angle is negligible.

Generalised stress intensity factors are reported in a number of papers (Gross and Mendelson [3], Zhao and Hahn [25], Chen [26], Dunn et al. [8,9], Lazzarin and Tovo [14], Atzori et al. [27], Strandberg [28,29], Noda and Takase [30]). In particular the accurate numerical results obtained by Noda and Takase by using the body force method will be reconsidered in the present paper with reference to a round bar under torsion.

Nowadays, the practice is to use systematically the numerical methods, independently of the complexity of the geometry. Numerical methods lead to sparse data, which are much less manageable than analytical results and sometimes make uneasy the understanding of the role played by all the involved geometrical parameters (Xu et al. [31]). For these reasons, analytical expressions, even when approximated, remain strongly desirable, also because they permit to reconsider the analytical basis of some fundamental contributions to the notch mechanics.

Differently from the theoretical stress concentration factor K_t, which can be applied only to blunt notches, the NSIFs can be applied both to sharp and blunt notches. Irwin [32] gave a fundamental relationship between the mode I SIF and the maximum stress at the tip of a blunt crack, $K_I = \sigma_{max}\sqrt{\pi\rho}/2$. Some years later, dealing with notches under mode I loading, this fundamental relationship was introduced by Glinka in Creager–Paris' solution [33,34] providing a bridging between LEFM and linear elastic notch mechanics. This close link was underlined also by Hasebe and Kutanda [35], who were able to demonstrate that the mode I SIF of an edge crack can be obtained from the stress distributions related to a semi-elliptic edge notch, in the presence of a notch radius to a notch depth ratio tending to zero.

An analytical frame for cracks, sharp and blunt U- and V-notches was proposed by Lazzarin and Tovo [36]. Some well known solutions due to Westergaard [1], Williams [2] and Creager–Paris [33] could be easily derived as special cases of that more general solution. Based on an improved version of that analytical frame, (see Filippi et al. [37]), some relationship linking the mode I NSIF of a blunt V-notch to the maximum stress at notch tip, such as to the NSIF of the corresponding sharp notch case were provided by Lazzarin and Filippi [38].

Independently, an analytical frame has been proposed for semi-elliptic notches (Lazzarin et al. [39]) as well as for parabolic or hyperbolic notches (Zappalorto et al. [40]) under torsion and uniform antiplane shear. This last paper represents the starting point of the present contribution mainly focused on the determination of analytical expressions for the mode III notch stress intensity factors for circumferentially-sharply-notched rounded bards under torsion loading, just starting from the theoretical stress distributions of the corresponding notch problem.

In more detail, the aims of the present work can be drawn as follows:

- To show that from a theoretically point of view the mode III NSIFs for a sharp notch can be determined from the theoretical stress concentration factor of the hyperbolic notch by imposing the limit condition of notch root radius tending to zero.
- To give closed-form expressions for NSIFs in the case of deep circumferential sharp V notches and discuss their range of applicability as a function of the opening angle 2α and the notch depth to the net radius ratio, R/a.
- To extend these expressions to a finite size body, by taking advantage of a shape function depending on the notch opening angle, 2α, and on the notch depth to the net radius ratio, R/a.

2. The stress intensity factor for circumferentially-cracked rounded bars under torsion loading

The mode I stress intensity factor for a crack of semi-length a in an infinite plate can be obtained by means of the following relationship [32]:

$$K_I = \lim_{\rho\to 0}\sigma_{max}\frac{\sqrt{\pi\rho}}{2} = \lim_{\rho\to 0}K_t\sigma_n\frac{\sqrt{\pi\rho}}{2} = \sqrt{\pi a}\sigma_n \tag{1}$$

by simply substituting the expression of the theoretical stress concentration factor valid for a slim elliptic notch, $K_t = 1 + 2\sqrt{a/\rho} \cong 2\sqrt{a/\rho}$ [41,42].

A relationship linking the maximum shear stress at the notch tip and the notch stress intensity factor for a blunt notch under torsion was provided by Hasebe and Kutanda [35]

$$K_{3,\rho} = \tau_{max}\sqrt{\pi\rho} \tag{2}$$

From a theoretical point of view, this expression is valid only for a parabolic notch, but it was shown that it can be successfully applied also to a degenerating-to-crack-semi-elliptic notch in an infinite shaft. This is because the stress distribution due to a semi-elliptic notch exactly tends to that of a parabolic notch [40]. The relevant mode III SIF turns out to be

$$K_{III} = \lim_{\rho\to 0}(\tau_{max}\sqrt{\pi\rho}) = \lim_{\rho\to 0}(\tau_n K_t\sqrt{\pi\rho}) = \tau_n\lim_{\rho\to 0}\left(\left(1+\sqrt{\frac{a}{\rho}}\right)\sqrt{\pi\rho}\right) = \tau_n\sqrt{\pi a} \tag{3}$$

Note also that, differently from mode I loading, no shape factor appears in the expression for K_{III} as due to the edge effect.

Consider now the solution obtain for a deep hyperbolic notch with a notch root radius ρ and a radius of the net section equal to R [42]

$$K_{tn} = \frac{3}{4}\frac{\left(\frac{R}{\rho}\right)^2}{2\left(\frac{R}{\rho}+1\right)\cdot\left(\sqrt{\frac{R}{\rho}}+1-1\right)-\frac{R}{\rho}} \tag{4}$$

This solution has been obtained by using the hyperbolic transformation $z = c\cos h\,\zeta$ (where $z = x + iy$ and $\zeta = \xi + i\eta$ are complex variables in the physical and the transformed planes, respectively, and c is a real number related to the focus of the

hyperbola), which results in a notch opening angle variable along the free edge. The angle of the asymptotes depends on ρ and R according to the following relationship:

$$\eta_0 = \arctan\sqrt{\frac{\rho}{R}} \tag{5}$$

However, when $\rho \to 0$, $\eta_0 = 0$, and the transformation gives a deep crack and never a pointed V-notch (for more details, see Ref. [40]). Then, by using Eq. (2), one obtains

$$K_{III} = \lim_{\rho\to 0}(\tau_{max}\sqrt{\pi\rho}) = \lim_{\rho\to 0}(\tau_n K_{tn}\sqrt{\pi\rho}) = \tau_n \lim_{\rho\to 0}\left(\frac{3}{4}\frac{\left(\frac{R}{\rho}\right)^2}{2\left(\frac{R}{\rho}+1\right)\cdot\left(\sqrt{\frac{R}{\rho}}+1-1\right)-\frac{R}{\rho}}\sqrt{\pi\rho}\right)$$
$$= \frac{3}{8}\tau_n\sqrt{\pi R} \cong 0.6647\times\tau_n\sqrt{R} \tag{6}$$

With reference to Fig. 1, when both a and R assumes finite values, K_{III} can be determined by means of the expression [21,43]

$$K_{III} = \tau_n\frac{3}{8}\sqrt{\pi R(1-\lambda)}\left[1+\frac{1}{2}\lambda+\frac{3}{8}\lambda^2+\frac{5}{16}\lambda^3+\frac{35}{128}\lambda^4+0.208\lambda^5\right] = \tau_n\frac{3}{8}\sqrt{\pi R(1-\lambda)}\cdot f_{B-K} \tag{7a}$$

where $\lambda = \frac{R}{R+a}$ and f_{B-K} matches the expression between the square brackets.

Eq. (7a) has found to be accurate within 3% [21,30]. The accuracy was further increased by Noda and Takase who proposed a modified version of Eq. (7a) [30]

$$K_{III} = \tau_n\frac{3}{8}\sqrt{\pi R(1-\lambda)}\cdot f_{B-K}\cdot(1.009-0.19064\cdot\varepsilon+1.2326\cdot\varepsilon^2-2.7484\cdot\varepsilon^3+2.7081\cdot\varepsilon^4-1.0024\cdot\varepsilon^5) \tag{7b}$$

where now $\varepsilon = \frac{a}{R+a}$.

3. Analytical solutions for the notch stress intensity factors due to deep sharp V-notches under torsion

3.1. Solid section

Dealing with V-notches, where the influence of the opening angle is crucial, a convenient expression for the mode III NSIF is [40]

$$K_{3,\rho} = \tau_{max}\sqrt{2\pi}r_0^{1-\lambda_3} \tag{8}$$

which is based on the stress distribution due to a hyperbolic notch. Then, differently from Eq. (2), Eq. (8) accounts for the influence of the notch opening angle. Here r_0 is the distance between the focus of the hyperbola (see Fig. 2) and the notch tip, whereas λ_3 is the eigenvalue of the corresponding sharp V-notch. The expression for the distance r_0 is [42]

$$r_0 = \frac{q-1}{q}\rho \tag{9}$$

where q depends on the asymptotic angle of the hyperbola, $2\alpha(\pi q = 2\pi - 2\alpha)$. The expression for λ_3 is [4–6]

$$\lambda_3 = \frac{1}{q} = \frac{\pi}{2(\pi-\alpha)} \tag{10}$$

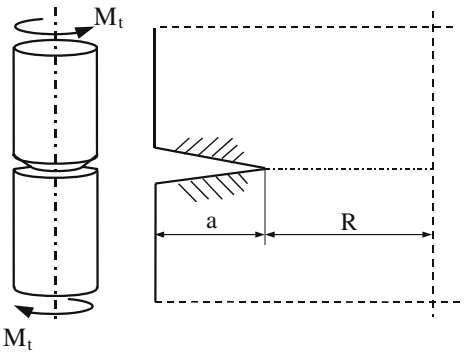

Fig. 1. Cracked bar under torsion load with net radius R and crack depth a; 3D view (a) and cross sectional view (b).

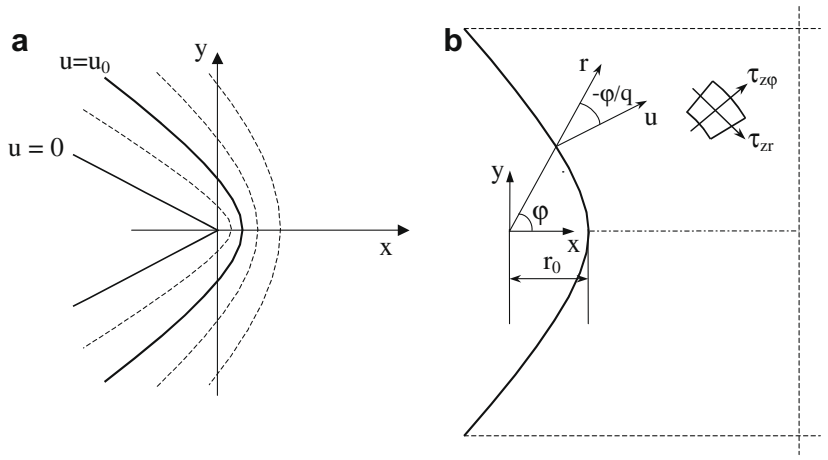

Fig. 2. (a) Auxiliary system of curvilinear coordinates (u, v); (b) reference system adopted for the solution.

It is, however, worth noting that when $2\alpha = 0$, $r_0 = \rho/2$ and $\lambda_3 = 0.5$, so that Eq. (8) matches Eq. (2).

The theoretical stress concentration factor for a deep hyperbolic notch in a rounded bar under torsion turns out to be (see Appendix A) [40]

$$K_{\mathrm{tn}} = \frac{s_3^4 + 10s_3^3 + 35s_3^2 + 50s_3 + 24}{4\sum_{j=0}^{3} I_j} \tag{11}$$

where $s_3 = \lambda_3 - 1 = (\alpha - \pi/2)/(\pi - \alpha)$ whereas the coefficients I_j have the close-form expressions reported in Appendix A.

Consider now a circumferential pointed V-notch in a rounded bar under torsion loading (see Fig. 3). The mode III linear elastic NSIF is defined as [44]

$$K_3^{\mathrm{V}} = \sqrt{2\pi} \lim_{r\to 0} r^{1-\lambda_3} \tau_{zy}(r, \varphi = 0) \tag{12}$$

to be seen as a natural extension of Gross and Mendelson's definitions for mode I and mode II NSIFs.

Then the expression of the elastic shear peak stress for hyperbolic notches can be used to estimate the NSIF of a sharp V-notch. Taking advantage of Eq. (8)

$$K_3^{\mathrm{V}} = \lim_{\rho\to 0} \tau_{\max} \sqrt{2\pi} r_0^{1-\lambda_3} = \sqrt{2\pi}\tau_{\mathrm{n}} \lim_{\rho\to 0} K_{\mathrm{tn}} r_0^{1-\lambda_3} = \sqrt{2\pi}\tau_{\mathrm{n}} \lim_{\rho\to 0} K_{\mathrm{tn}} r_0^{-s_3} \tag{13}$$

$$\lim_{\rho\to 0} K_{\mathrm{tn}} r_0^{-s_3} = \frac{(s_3^4 + 10s_3^3 + 35s_3^2 + 50s_3 + 24)}{4} \cdot \lim_{\rho\to 0} \frac{1}{\sum_{j=0}^{3} I_j r_0^{s_3}} \tag{14}$$

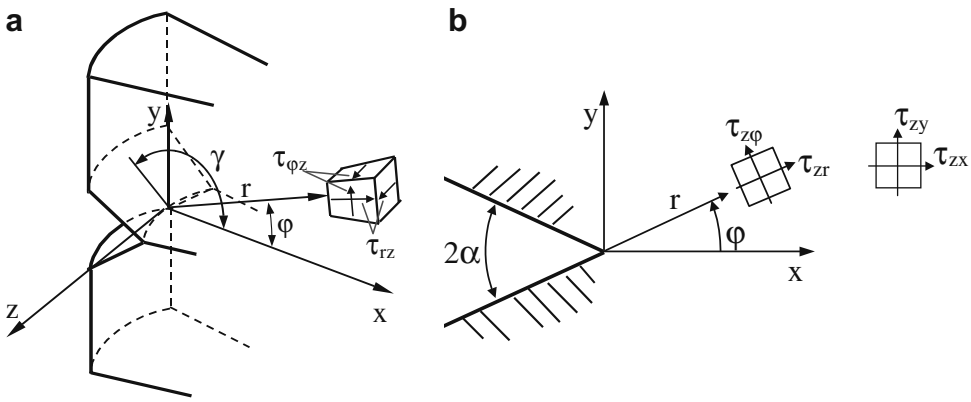

Fig. 3. V-notched rounded bar under torsion; 3D view (a) and cross sectional view (b).

Considering one by one the terms on the right hand side of Eq. (14), we have

$$\lim_{\rho\to 0} I_0 r_0^{s_3} = \lim_{k\to 0} R^{s_3}(6+24k+36k^2+24k^3+6k^4) = 6R^{s_3} \tag{15}$$

$$\lim_{\rho\to 0} I_1 r_0^{s_3} = \lim_{r_0\to 0} -\frac{r_0^{1+s_3}}{R}(24+26s_3+9s_3^2+s_3^3+24) \propto \lim_{r_0\to 0} -\frac{r_0^{\lambda_3}}{R} = 0 \tag{16}$$

$$\lim_{\rho\to 0} I_2 r_0^{s_3} = \lim_{r_0\to 0} -\frac{r_0^{2+s_3}}{R^2}(36+21s_3+3s_3^2) = 0 \tag{17}$$

$$\lim_{\rho\to 0} I_2 r_0^{s_3} = \lim_{r_0\to 0}\left[-\frac{r_0^{3+s_3}}{R^3}(24+6s_3) - 6\frac{r_0^{4+s_3}}{R^4}\right] = 0 \tag{18}$$

Then it is easy to obtain the expression of the NSIF normalised with respect to the nominal shear stress on the net sectional area

$$\bar{K}_3^{\mathrm{V}} = \frac{K_3^{\mathrm{V}}}{\tau_{\mathrm{n}}} = \sqrt{2\pi}\frac{s_3^4+10s_3^3+35s_3^2+50s_3+24}{24}R^{1-\lambda_3} \tag{19}$$

as well as the non-dimensional shape factor $k_{3\mathrm{d}}$

$$k_{3\mathrm{d}} = \frac{\bar{K}_3^{\mathrm{V}}}{R^{1-\lambda_3}} = \sqrt{2\pi}\frac{s_3^4+10s_3^3+35s_3^2+50s_3+24}{24} \tag{20}$$

where the subscript 'd' means 'deep'.

Eq. (20) is plotted in Fig. 4 as a function of the notch opening angle.

By a mathematical point of view, this plot is valid only for a semi-infinite V-notch, but it will be shown in Section 7 that Eq. (20) can be applied as it stands also in many cases of practical interest.

It is also interesting to note that for the crack case, $2\alpha = 0$, Eq. (20) leads to

$$k_{\mathrm{IIId}} = \frac{105}{384}\sqrt{2\pi} \cong 0.68541 \tag{21}$$

the difference being within 3% with respect to Eq. (6). This difference is due to the different shape of the initial notch (deep hyperbolic notch against deep parabolic notch). Even if no explicit comparison is carried out here, it is useful to remember that cracked bars under torsion were analysed also by Chen et al. [45] by using a dual integration formulation combined with the boundary element method.

3.2. Hollow section

By proceeding in the same way, one obtains the following expressions for the theoretical stress concentration factor for a hollow section:

$$K_{\mathrm{tn}} = \frac{(1-\kappa_2^4)(s_3^4+10s_3^3+35s_3^2+50s_3+24)}{4(I_1+I_2)} \tag{22}$$

where all the involved parameters are reported in Appendix A.

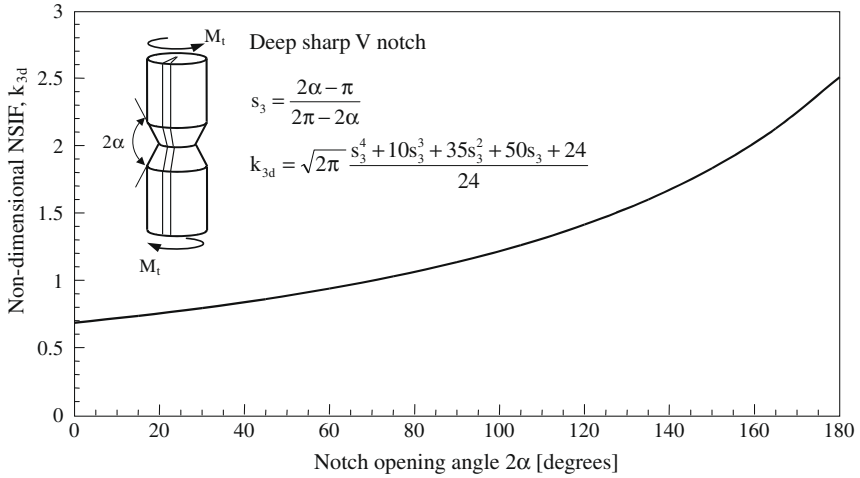

Fig. 4. Non-dimensional NSIF for deep notches as a function of the notch opening angle 2α.

Then, by means of Eq. (8) one obtains the following expression for the NSIFs normalised with respect to the nominal shear stress on net sectional area:

$$\bar{K}_3^{V} = \sqrt{2\pi}\frac{(1-\kappa_2^4)(s_3^4+10s_3^3+35s_3^2+50s_3+24)}{4(1-\kappa_2)^{1+s_3}[6+6\kappa_2(1+s_3)+3\kappa_2^2(2+3s_3+s_3^2)+\kappa_2^3(6+11s_3+6s_3^2+s_3^3)]}R^{1-\lambda_3} \tag{23}$$

as well as for the non-dimensional parameter

$$k_{3h} = \frac{\bar{K}_3^{V}}{R^{1-\lambda_3}} = \sqrt{2\pi}\frac{(1-\kappa_2^4)(s_3^4+10s_3^3+35s_3^2+50s_3+24)}{4(1-\kappa_2)^{1+s_3}[6+6\kappa_2(1+s_3)+3\kappa_2^2(2+3s_3+s_3^2)+\kappa_2^3(6+11s_3+6s_3^2+s_3^3)]} \tag{24}$$

Note that, if $R_i = 0$, then $\kappa_2 = 0$, and Eqs. (23) and (24) matches Eqs. (19) and (20), respectively.

4. Notch stress intensity factors for shallow sharp V-notches in solid bars under torsion

Since, except for the crack case, a complete analytical solution for the problem of a shallow sharp V-notch seems to be far from easy, the solution has been obtained here by means of some finite element analyses. Six notch opening angles have been considered, namely 30°, 60°, 90°, 120°, 135° and 150°, with a ratio R/a equal to 10^4. When the notch is shallow with respect to the net section, the absolute dimensions can be given in terms of the notch depth a. Then

$$\bar{K}_3^{V} = k_{3s}a^{1-\lambda_3} \tag{25}$$

Values of k_{3s} for the analysed notch opening angles are reported in Fig. 5. It has been found that a good approximation (within 1%) can be achieved by means of the following polynomial expression:

$$k_{3s} = \sqrt{\pi}\left(-\frac{3779}{878}\cdot s_3^2 - \frac{90}{119}\cdot s_3 + \frac{527}{312}\right). \tag{26}$$

5. Notch stress intensity factors for finite sharp V-notches in solid bars under torsion

In general, for rounded bar of finite size Eq. (19) needs to be updated by introducing a dimensionless factor k_3 that depends not only on the notch opening angle but also on the ratio R/a, where a is the notch depth and R the radius of the net transverse section, so that

$$\bar{K}_3^{V} = k_3 R^{1-\lambda_3} \tag{27}$$

The shape factor k_3 $(2\alpha, R/a)$ has been determined by fitting more than two hundred FE analyses carried out with the Ansys 9.0 code. In practice, for most of applications, the range $1 \leqslant R/a \leqslant 20$ is useful. Accurate expressions for k_3 within this range can be obtained by using a quadratic polynomials and are listed in Table 1 and plotted in Fig. 6 as functions of the notch opening angle.

In this work a wider range has also been considered, namely $1 \leqslant R/a \leqslant 100$; in this case, however, the best fitting polynomials are much more complicated and are reported for the sake of completeness in Appendix B.

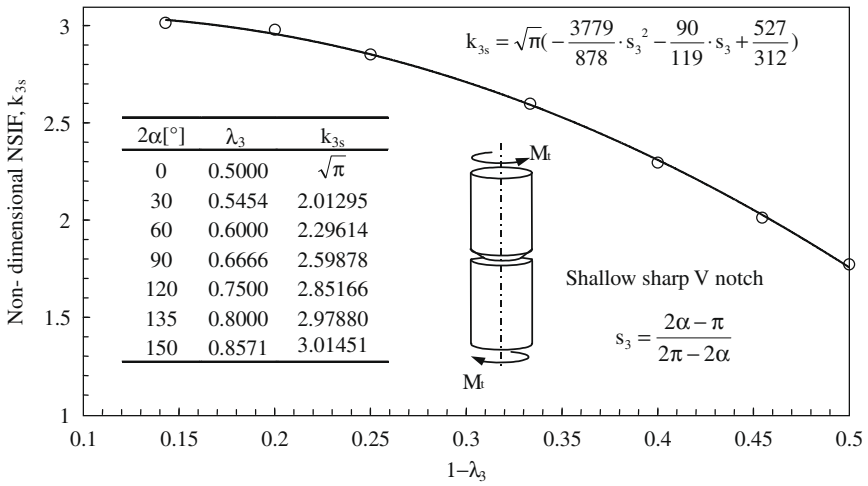

Fig. 5. Non-dimensional NSIF for shallow sharp notches as a function of $1 - \lambda_3$.

Table 1
Expressions for the non-dimensional NSIF, k_3, within the range $1 \leqslant R/a \leqslant 20$.

2α (°)	$k_3(2\alpha, \psi = R/a)$	2α (°)	$k_3(2\alpha, \psi = R/a)$
30	$\frac{17}{3}\cdot 10^{-4}\psi^2 - \frac{63}{22}\cdot 10^{-2}\psi + \frac{47}{58}$	120	$\frac{7}{39}\cdot 10^{-4}\psi^2 - \frac{29}{23}\cdot 10^{-2}\psi + \frac{116}{79}$
60	$\frac{437}{99}\cdot 10^{-4}\psi^2 - \frac{155}{59}\cdot 10^{-2}\psi + \frac{94}{97}$	135	$-\frac{27}{28}\cdot 10^{-4}\psi^2 - \frac{11}{16}\cdot 10^{-2}\psi + \frac{104}{63}$
90	$\frac{147}{55}\cdot 10^{-4}\psi^2 - \frac{63}{29}\cdot 10^{-2}\psi + \frac{45}{38}$	150	$-\frac{4}{3}\cdot 10^{-4}\psi^2 - \frac{16}{85}\cdot 10^{-2}\psi + \frac{118}{63}$

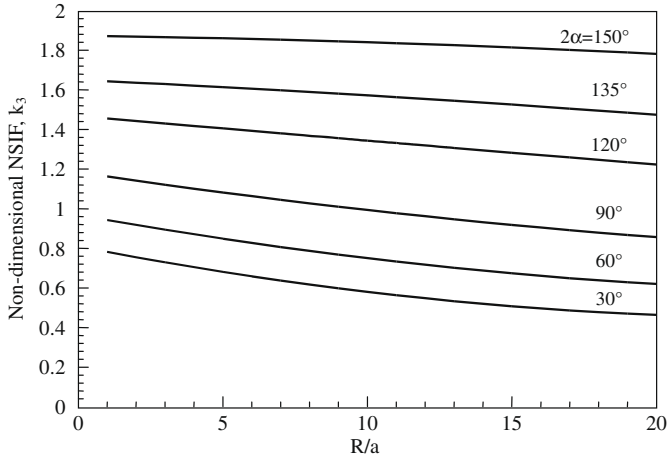

Fig. 6. Plots of the non-dimensional parameter k_3 for different opening angles as a function of R/a.

Since for small variations of λ_3 the trend of k_3 is approximately linear, the values of k_3 for a general notch opening angle 2α between those analysed here can be determined by using the following linear rule:

$$k_{3,2\alpha} = k_{3,2\alpha_1} + \frac{k_{3,2\alpha_2} - k_{3,2\alpha_1}}{\lambda_{3,2\alpha_2} - \lambda_{3,2\alpha_1}}(\lambda_{3,2\alpha} - \lambda_{3,2\alpha_1}) \tag{28}$$

with $\alpha_1 < \alpha < \alpha_2$.

Then, if one knows the k_3 values, related to a given R/a ratio, for two notch opening angles, $2\alpha_1$ and $2\alpha_2$, the values of k_3 for the same R/a ratio but for an opening angle 2α (such that $2\alpha_1 < 2\alpha < 2\alpha_2$) can be approximately obtained by applying Eq. (28).

6. Comparison with the results by Noda and Takase

6.1. Shallow notches

Recently Noda and Takase [30], dealing with shallow notches under torsion, reported for some notch opening angles the values of the shape function F_{IIIs}, being $k_{3s} = F_{\mathrm{IIIs}}\sqrt{\pi}$.

An explicit comparison between the values for F_{IIIs} provided by Noda and Takase (*ibid*. Table 3, [30]) and those obtained in this work is reported in Table 2. It is important to note that the definition of the mode III NSIF given by Noda and Takase is different than that of the present paper, Eq. (12). The comparison is then carried out between F_{IIIs} provided by Eq. (26) and $F^{\mathrm{ref}}_{\mathrm{IIIs}}$, defined as follows:

$$F^{\mathrm{ref}}_{\mathrm{IIIs}} = \frac{\pi\cos(\lambda_3\alpha)}{\pi - \alpha}F^{\mathrm{Noda-Takase}}_{\mathrm{IIIs}}. \tag{29}$$

6.2. Deep notches and finite notches

For a wide number of a/R_{gross} values, Noda and Takase also provided the ratio $\eta = F_{\mathrm{III}}/F_{\mathrm{IIIs}}$, where F_{IIIs} is the shape function of the shallow notch (namely of the notch in an infinite body) and F_{III} is the shape function of the notch of arbitrary depth. Then [30]

$$\bar{K}^{\mathrm{V}}_3 = F_{\mathrm{III}}\sqrt{\pi}a^{1-\lambda_3} \quad F_{\mathrm{III}} = \eta F_{\mathrm{IIIs}} \tag{30a–b}$$

By comparing Eqs. (27) and (30a) one obtains

Table 2
Comparison between F^{ref}_{IIIs} for shallow notches as obtained by Noda and Takase [30] and F_{IIIs} according to this work.

2α (°)	$1-\lambda_3$	F^{ref}_{IIIs} [a]	F_{IIIs} [b]	Δ (%)
0	1/2	1	1	0.00
30	5/11	1.1382	1.1357	0.22
60	2/5	1.2957	1.2955	0.02
90	1/3	1.4655	1.4662	−0.05

[a] According to Eq. (29).
[b] $F_{IIIs} = k_{3s}/\sqrt{\pi}$, with k_{3s} according to the present work.

Table 3
Comparison between F^{ref}_{III} as obtained by Noda and Takase [30] and F_{III} according to this work.

2α (°)	a/R_{gross}	a/R	η	F_{III}	F^{ref}_{III}	Δ (%)
30	0.01	0.0101	0.979	1.11392	1.11432	−0.0
	0.02	0.0204	0.957	1.0911	1.08928	0.2
	0.05	0.0526	0.895	1.01344	1.01871	−0.52
	0.1	0.1111	0.806	0.91453	0.91741	−0.3
	0.2	0.2500	0.664	0.74401	0.75578	−1.6
	0.3	0.4286	0.554	0.61903	0.63058	−1.8
	0.4	0.6667	0.465	0.52279	0.52927	−1.2
	0.5	1.0000	0.391	0.44337	0.44505	−0.4
	0.6	1.5000	0.327	0.37283	0.37220	0.2
	0.7	2.3333	0.268	0.305	0.30504	−0.0
	0.8	4.0000	0.209	0.23872	0.23789	0.3
	0.9	9.0000	0.145	0.16512	0.16504	0.1
60	0.01	0.0101	0.978	1.26883	1.26718	0.1
	0.02	0.0204	0.956	1.24133	1.23867	0.2
	0.05	0.0526	0.895	1.15589	1.15963	−0.3
	0.1	0.1111	0.807	1.04247	1.04561	−0.3
	0.2	0.2500	0.67	0.85407	0.86811	−1.6
	0.3	0.4286	0.565	0.72067	0.73206	−1.5
	0.4	0.6667	0.482	0.61836	0.62452	−0.9
	0.5	1.0000	0.412	0.53341	0.53382	−0.1
	0.6	1.5000	0.351	0.45021	0.45478	−1.0
	0.7	2.3333	0.295	0.37728	0.38223	−1.3
	0.8	4.0000	0.237	0.30411	0.30708	−0.9
	0.9	9.0000	0.172	0.21986	0.22286	−1.3
90	0.01	0.0101	0.977	1.44298	1.43184	0.8
	0.02	0.0204	0.955	1.40234	1.3996	0.2
	0.05	0.0526	0.895	1.31037	1.31166	−0.1
	0.1	0.1111	0.81	1.18453	1.18709	−0.2
	0.2	0.2500	0.681	0.9857	0.99804	−1.2
	0.3	0.4286	0.585	0.84879	0.85734	−1.0
	0.4	0.6667	0.509	0.74381	0.74596	−0.3
	0.5	1.0000	0.446	0.65578	0.65363	0.3
	0.6	1.5000	0.39	0.55925	0.57156	−2.1
	0.7	2.3333	0.336	0.48266	0.49242	−1.9
	0.8	4.0000	0.281	0.40329	0.41182	−2.0
	0.9	9.0000	0.214	0.30777	0.31363	−1.9

Relative deviations determined according to the following expression: $\Delta[\%] = \frac{F_{III}-F^{ref}_{III}}{F^{ref}_{III}} \cdot 100$.

$$k_3 = F_{III}\sqrt{\pi}\left(\frac{a}{R}\right)^{1-\lambda_3} \tag{31}$$

or vice versa

$$F_{III} = \left(\frac{R}{a}\right)^{1-\lambda_3} \cdot k_3/\sqrt{\pi} \tag{32}$$

Thus, we can compare our results with those by Noda and Takase. In particular in Table 3, two different values for F_{III} are compared:

- F_{III}, obtained by using Eq. (32). Here k_3 has been determined by means of the expressions reported in Table 1 when $1 < R/a < 20$, in Table B1 (Appendix B) when $R/a > 20$ or according to Eq. (20), valid for deep notches, when $R/a < 1$.

- F_{III}^{ref}, obtained by using (30b) with $F_{IIIs} = F_{IIIs}^{ref}$, as obtained from Eq. (29), and η according to Noda and Takase (*ibid.* Table 9, [30]).

It is evident that the agreement is very good (the maximum difference being 2%).

7. Results of Fe analyses and final discussion

Figs. 7–10 show a comparison between Eqs. (19) and (27) and numerical results; as it can be seen, the agreement with the theoretical prediction is very satisfactory. It is also evident that while Eq. (27), which includes the shape function, is accurate on the entire considered domain, the range of validity of Eq. (19), which is fully analytical and valid for deep notches, changes as a function of the notch opening angle 2α. In particular the range of validity increases as the notch opening angle increases. For example to get an error, with respect to the results of finite element analyses, less than 4% it is necessary that the R/a ratio is less than or equal to 3 for $2\alpha = 60°$, 9 for $2\alpha = 120°$ and 15 for $2\alpha = 135°$.

Finally, Fig. 10 show a comparison between $\bar{K}_3^V$ for different notch opening angles with $a = 10$ mm, the crack case being included. It is also evident that Eq. (7b) proposed by Noda and Takase works very well.

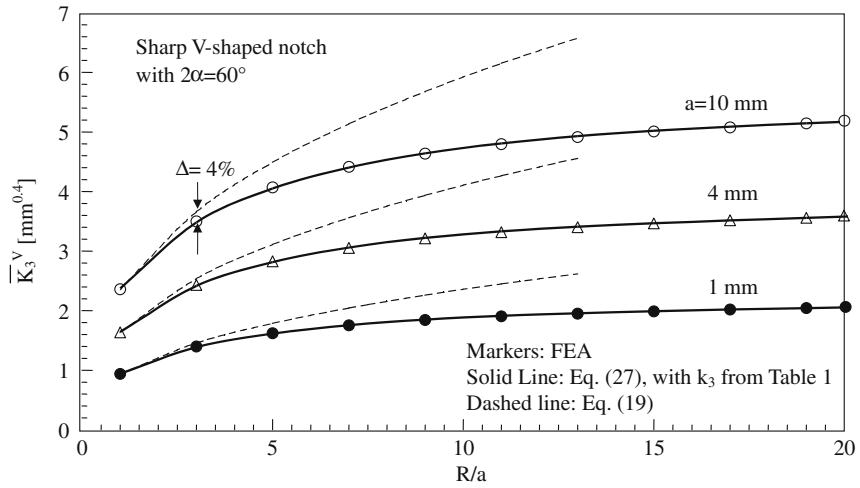

Fig. 7. Comparison between Eqs. (19) and (27) and numerical results as a function of R/a. Notch opening angle $2\alpha = 60°$.

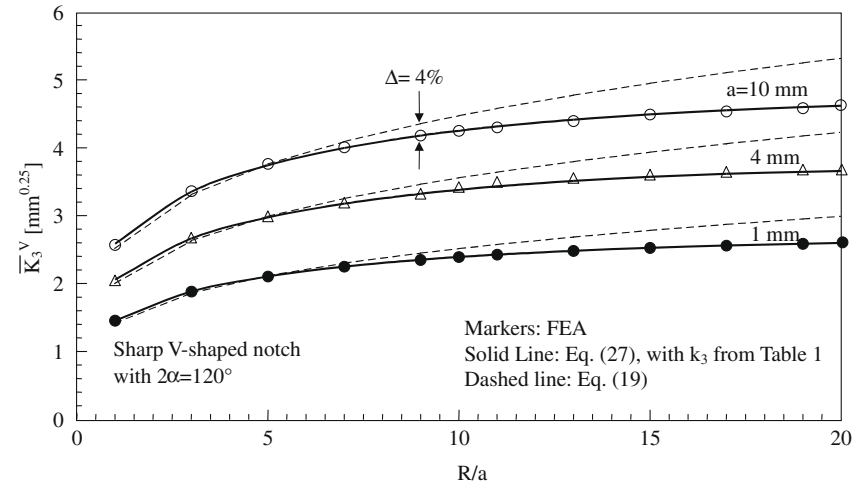

Fig. 8. Comparison between Eqs. (19) and (27) and numerical results as a function of R/a. Notch opening angle $2\alpha = 120°$.

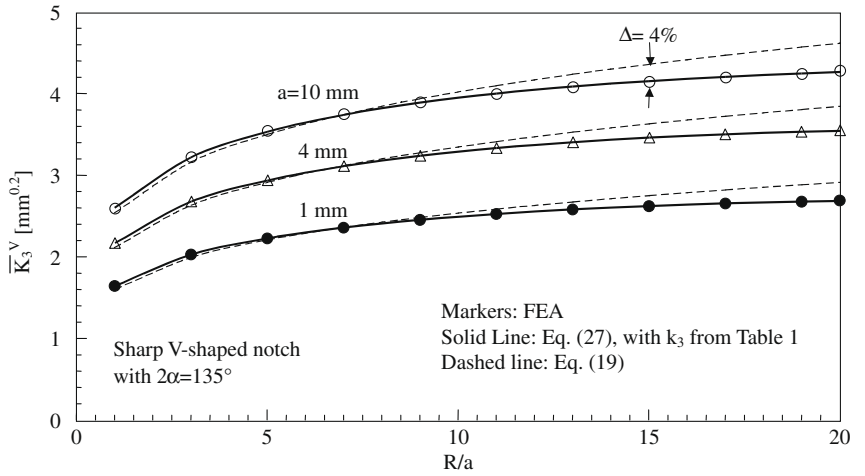

Fig. 9. Comparison between Eqs. (19) and (27) and numerical results as a function of R/a. Notch opening angle $2\alpha = 135°$.

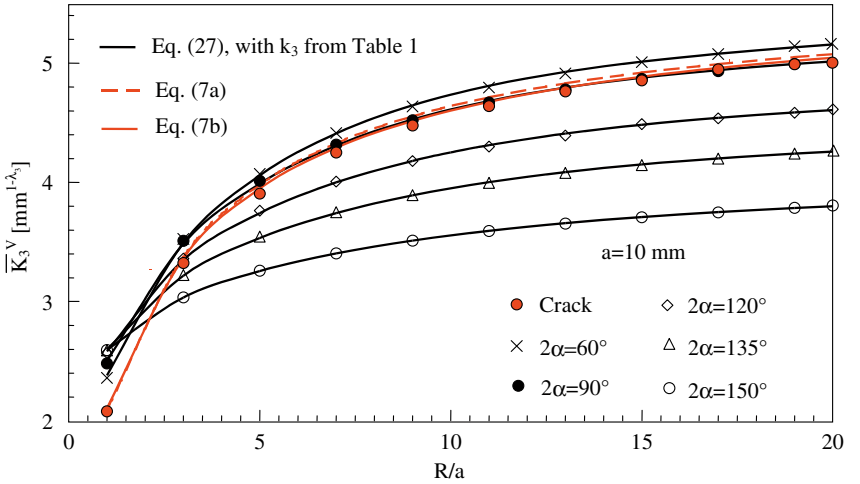

Fig. 10. Comparison between Eqs. (7a), (7b), and (27) and numerical results, with notch depth $a = 10$ mm and notch opening angle 2α.

8. Conclusion

Analytical expressions for the notch stress intensity factors as due to deep circumferential sharp V-notches under torsion loading have been found starting from the expressions of the theoretical stress concentration factor of a hyperbolic notch. The hyperbolic notch allows us to account for the influence of the V-notch opening angle, which is not included when a parabolic notch is considered.

The work confirms the existence of an explicit analytical link between the theoretical stress concentration factor for a notch and the notch stress intensity factor of the corresponding sharp V-notch feature, that are, instead, by a theoretical point of view often thought as different and independent.

By staring from these analytical bases, the expressions have been improved to account for the finite dimension of the notch. Simple practical expressions have been determined by means of a numerical best fitting procedure, which have been proved to be in good agreement with the results of a large body of finite element analyses.

Appendix A. Closed-form solutions of stress distributions for hyperbolic and parabolic notches

Consider the following transformation [42]:

$$z = w^q \tag{A.1}$$

Where $z = x + iy$ and $w = u + iv$ are complex variables in the physical and the transformed planes, respectively, and q is a real number related to the opening angle of the curve 2α:

$$q = \frac{2\pi - 2\alpha}{\pi} = \frac{2\gamma}{\pi} \tag{A.2}$$

The curvilinear coordinate system introduced here allows one to completely describe the hyperbolic ($1 < q < 2$) or parabolic ($q = 2$) profiles (see Fig. 2).

Stress distributions ahead of the notch can be determined by using the following complex potential:

$$H(z) = Az^{\lambda_3} \tag{A.3}$$

being λ_3 a real number and A a complex coefficient.Then, it is possible to write [40]

$$\begin{aligned}\tau_{zr} &= \mathrm{Re}\{e^{i\varphi}H'(z)\} = \lambda_3 r^{\lambda_3-1}(-A_2\sin\lambda_3\varphi + A_1\cos\lambda_3\varphi)\\ \tau_{z\varphi} &= -\mathrm{Im}\{e^{i\varphi}H'(z)\} = \lambda_3 r^{\lambda_3-1}(-A_1\sin\lambda_3\varphi - A_2\cos\lambda_3\varphi)\end{aligned} \tag{A.4}$$

At $r \to \infty$ the conic defined by $u = u_0$ presents the same inclination of the flanks of the V-notch with the same opening angle, which, from a mathematical point of view, represent the two asymptotes; then

$$\lim_{\substack{r\to+\infty\\ \varphi\to\pm\gamma}} (r^{1-\lambda_3}\tau_{z\varphi}) = 0 \tag{A.5}$$

giving the following system:

$$\begin{bmatrix} \sin\lambda_3\gamma & \cos\lambda_3\gamma \\ -\sin\lambda_3\gamma & \cos\lambda_3\gamma \end{bmatrix} \begin{Bmatrix} A_1 \\ A_2 \end{Bmatrix} = \underline{0} \tag{A.6}$$

whose solutions gives, considering only the smaller positive value of λ_3

$$\lambda_3 = \frac{\pi}{2\gamma} = \frac{1}{q} \quad A_1 = -A_2 \cdot \frac{\cos\lambda_3\gamma}{\sin\lambda_3\gamma} = -A_2 \cdot \frac{\cos(\pi/2)}{\sin(\pi/2)} = 0 \tag{A.7}$$

The coefficient A_2 can be determined as a function of the maximum shear stress occurring at the notch tip

$$A_2 = \frac{-\tau_{\max}}{\lambda_3 r_0^{\lambda_3-1}} \tag{A.8}$$

so that, finally [40]

$$\begin{Bmatrix} \tau_{zr}(r,\varphi) \\ \tau_{z\varphi}(r,\varphi) \end{Bmatrix} = \tau_{\max}\left(\frac{r}{r_0}\right)^{\lambda_3-1} \begin{Bmatrix} \sin\lambda_3\varphi \\ \cos\lambda_3\varphi \end{Bmatrix} \tag{A.9}$$

Extending the NSIF definitions from the plane problems to the antiplane case gives

$$K_{3,\rho} = \sqrt{2\pi}\lim_{r\to r_0^+}[r^{1-\lambda_3}\tau_{z\varphi}(r,\varphi=0)] \tag{A.10}$$

and the following relationship between the generalized stress intensity factor and the maximum shear stress holds valid:

$$K_{3,\rho} = \tau_{\max}\sqrt{2\pi}r_0^{1-\lambda_3} \tag{A.11}$$

Along the notch bisector line, it is possible to write

$$\tau_{z\varphi}\big|_{y=0} = \tau_{zy}\big|_{y=0} = \tau_{\max}\left(\frac{x}{r_0}\right)^{\lambda_3-1}\left(1 - \frac{x-r_0}{R}\right) \tag{A.12}$$

where the term $(1 - \frac{x-r_0}{R})$ is introduced here accounting for the linear decrease of the nominal shear stress.

By means of the following change of variable $t = R + r_0 - x$, we can write the equilibrium equation on the net section by equating the contribution given by the τ_{zy} stress and that due to the nominal shear stress τ_n, ranging from τ^* to 0

$$\int_0^{2\pi}\int_0^R \tau_n \frac{t^3}{R}\,\mathrm{d}t\,\mathrm{d}\theta = \int_0^{2\pi}\int_0^R \tau_{\max}\left(\frac{R+r_0-t}{r_0}\right)^{\lambda_3-1}\frac{t^3}{R}\,\mathrm{d}t\,\mathrm{d}\theta \tag{A.13}$$

so that, by means of some algebraic manipulations the stress concentration factor turns out to be [40]

$$K_{t_n} = \frac{s_3^4 + 10s_3^3 + 35s_3^2 + 50s_3 + 24}{4\sum_{j=0}^3 I_j} \tag{A.14}$$

where

$$
\begin{aligned}
&s_3 = s_3(2\alpha) = \lambda_3 - 1 \quad k = k(r_0, R) = \frac{r_0}{R} \\
&I_0 = \left(1 + \frac{1}{k}\right)^{s_3} [6 + 24k + 36k^2 + 24k^3 + 6k^4] \\
&I_1 = -k(24 + 26s_3 + 9s_3^2 + s_3^3) \\
&I_2 = -k^2(36 + 21s_3 + 3s_3^2) \\
&I_3 = -k^3(24 + 6s_3) - 6k^4
\end{aligned}
\tag{A.15}
$$

Consider now a hollow section (see Fig. A1), the expression for K_t becomes

$$
K_{t_n} = \frac{\frac{R_n^4}{4} - \frac{R_i^4}{4}}{\int_{R_i}^{R_n} \left(\frac{R_n + r_0 - t}{r_0}\right)^{\lambda_3 - 1} t^3 dt}
\tag{A.16}
$$

that is

$$
K_{t_n} = \frac{(1 - \kappa_2^4)(s_3^4 + 10s_3^3 + 35s_3^2 + 50s_3 + 24)}{4(I_1 + I_2)}
\tag{A.17}
$$

where

$$
\begin{aligned}
&s_3(2\alpha) = \lambda_3 - 1 \\
&\kappa_1(\rho, R) = \frac{r_0}{R_n} \\
&\kappa_2(\rho, R) = \frac{R_i}{R_n} \\
&I_1 = (1 + \kappa_1 - \kappa_2)\left(\frac{1 + \kappa_1 - \kappa_2}{\kappa_1}\right)^{s_3} \left[6(\kappa_1 + 1)^3 + 6\kappa_2(\kappa_1 + 1)^2(1 + s_3) + 3\kappa_2^2(\kappa_1 + 1)(2 + 3s_3 + s_3^2)\right. \\
&\quad \left. + \kappa_2^3(6 + 11s_3 + 6s_3^2 + s_3^3)\right] \\
&I_2 = -\kappa_1\left[6\kappa_1^3 + 6\kappa_1^2(4 + s_3) + 3\kappa_1(12 + 7s_3 + s_3^2) + 24 + 26s_3 + 9s_3^2 + s_3^3\right]
\end{aligned}
\tag{A.18}
$$

being R_n and R_i respectively the external and the internal radius of the net section (see Fig. A1)

Appendix B. Expressions for the non-dimensional NSIF k_3 within the range $1 \leqslant R/a \leqslant 100$

When $R/a > 20$ the quadratic polynomials given in Table 1 are not accurate enough and may cause unacceptable errors in the k_3 prediction, the entity of the error depending also on the notch opening angle. Then we have determined new expressions to fit numerical results on the wider range $1 \leq r/a \leq 100$, which are reported in Table B1. A comparison with numerical results is shown in Fig. B1.

Do note that, in the range $1 \leqslant R/a \leqslant 20$, the polynomials in Table 1 and those in Table B1 give results very closed to each other, with a maximum difference equal to 0.5% (see Table B2).

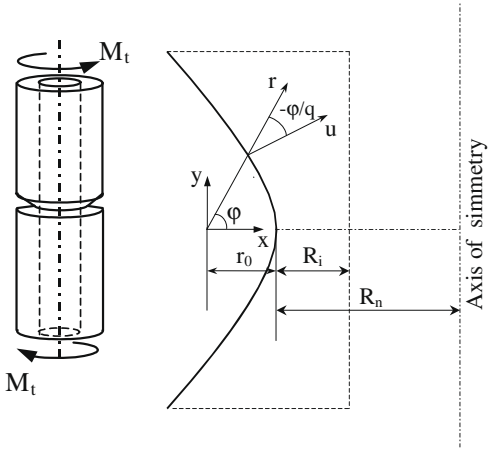

Fig. A1. Notched shaft with a hollow section.

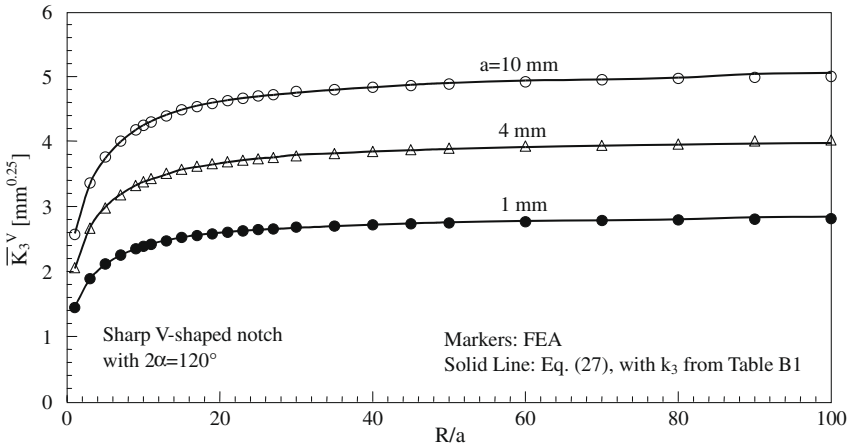

Fig. B1. Comparison between the NSIFs obtained by using the shape function in Table B1 and numerical results. Notch opening angle $2\alpha = 120°$, notch depth $a = 1, 4, 10$ mm.

Table B1
Expressions for the non-dimensional NSIF, k_3, within the range $1 \leqslant R/a \leqslant 100$.

2α (°)	$k_3(2\alpha, \psi = R/a)$
30	$5.1615 \cdot 10^{-12}\psi^6 - 1.9653 \cdot 10^{-9}\psi^5 + 3.0432 \cdot 10^{-7}\psi^4 - 2.4787 \cdot 10^{-5}\psi^3 + 1.1589 \cdot 10^{-3}\psi^2 - 3.3166 \cdot 10^{-2}\psi + 8.1788 \cdot 10^{-1}$
60	$-1.5077 \cdot 10^{-13}\psi^6 - 2.3723 \cdot 10^{-10}\psi^5 + 8.6554 \cdot 10^{-8}\psi^4 - 1.1460 \cdot 10^{-5}\psi^3 + 7.5995 \cdot 10^{-4}\psi^2 - 2.8903 \cdot 10^{-2}\psi + 9.7364 \cdot 10^{-1}$
90	$-5.4247 \cdot 10^{-12}\psi^6 + 1.5407 \cdot 10^{-9}\psi^5 - 1.4761 \cdot 10^{-7}\psi^4 + 3.7591 \cdot 10^{-6}\psi^3 + 2.5755 \cdot 10^{-4}\psi^2 - 2.1927 \cdot 10^{-2}\psi + 1.1844$
120	$-8.9846 \cdot 10^{-12}\psi^6 + 2.8405 \cdot 10^{-9}\psi^5 - 3.3822 \cdot 10^{-7}\psi^4 + 1.8076 \cdot 10^{-5}\psi^3 - 3.2136 \cdot 10^{-4}\psi^2 - 1.0370 \cdot 10^{-2}\psi + 1.4646$
135	$-9.7056 \cdot 10^{-12}\psi^6 + 3.1530 \cdot 10^{-9}\psi^5 - 3.9227 \cdot 10^{-7}\psi^4 + 2.2903 \cdot 10^{-5}\psi^3 - 5.6314 \cdot 10^{-4}\psi^2 - 3.5700 \cdot 10^{-3}\psi + 1.6452$
150	$-5.3293 \cdot 10^{-12}\psi^6 + 1.8081 \cdot 10^{-9}\psi^5 - 2.3952 \cdot 10^{-7}\psi^4 + 1.5445 \cdot 10^{-5}\psi^3 - 4.6399 \cdot 10^{-4}\psi^2 + 5.0719 \cdot 10^{-4}\psi + 1.8690$

Table B2
Comparison between predicted non-dimensional NSIFs within the range $1 \leqslant R/a \leqslant 20$.

2α (°)	R/a	k_3[a]	k_3[b]	Δ (%)	2α (°)	R/a	k_3[a]	k_3[b]	Δ (%)
30	20.00	0.4643	0.4625	0.4	120	20.00	1.2234	1.2281	−0.4
	10.00	0.5806	0.5802	0.1		10.00	1.3441	1.3441	0.0
	4.00	0.7049	0.7026	0.3		4.00	1.4182	1.4194	−0.1
	2.00	0.7553	0.7566	−0.2		2.00	1.4432	1.4431	0.0
	1.33	0.7732	0.7764	−0.4		1.33	1.4516	1.4506	0.1
	1.00	0.7823	0.7866	−0.5		1.00	1.4558	1.4543	0.1
60	20.00	0.6202	0.6210	−0.1	135	20.00	1.4747	1.4783	−0.2
	10.00	0.7505	0.7500	0.1		10.00	1.5724	1.5723	0.0
	4.00	0.8711	0.8695	0.2		4.00	1.6217	1.6231	−0.1
	2.00	0.9183	0.9188	−0.1		2.00	1.6367	1.6358	0.1
	1.33	0.9348	0.9364	−0.2		1.33	1.6415	1.6393	0.1
	1.00	0.9432	0.9455	−0.2		1.00	1.6438	1.6409	0.2
90	20.00	0.8566	0.8594	−0.3	150	20.00	1.7820	1.7843	−0.1
	10.00	0.9937	0.9929	0.1		10.00	1.8409	1.8409	0.0
	4.00	1.1016	1.1006	0.1		4.00	1.8633	1.8645	−0.1
	2.00	1.1418	1.1412	0.1		2.00	1.8687	1.8683	0.0
	1.33	1.1557	1.1552	0.0		1.33	1.8703	1.8689	0.1
	1.00	1.1627	1.1623	0.0		1.00	1.8710	1.8690	0.1

The variation in percent is determined according to the expression $\Delta = \lfloor (k_3^{(a)} - k_3^{(b)})/k_3^{(b)} \rfloor \times 100$.
[a] Determined by means of the polynomials of Table 1.
[b] By means of the polynomials of Table B1.

References

[1] Westergaard HM. Bearing pressures and cracks. J Appl Mech 1939;6:A49–53.
[2] Williams ML. Stress singularities resulting from various boundary conditions in angular corners of plate in extension. J Appl Mech 1952;19:526–8.
[3] Gross R, Mendelson A. Plane elastostatic analysis of V-notched plates. Int J Fract Mech 1972;8:267–76.
[4] Seweryn A, Molski K. Elastic stress singularities and corresponding generalized stress intensity factors for angular corners under various boundary condition. Engng Fract Mech 1996;55:529–56.

[5] Dunn ML, Suwito W, Cunningham S. Stress intensities at notch singularities. Engng Fract Mech 1997;57:417–30.
[6] Qian J, Hasebe N. Property of Eigenvalues and eigenfunctions for an interface V-notch in antiplane elasticity. Engng Fract Mech 1997;56:729–34.
[7] Nui LS, Chehimi C, Pluvinage G. Stress field near a large blunted tip V-notch and application of the concept of the critical notch stress intensity factor (NSIF) to the fracture toughness of very brittle materials. Engng Fract Mech 1994;49:325–35.
[8] Dunn ML, Suwito W, Cunningham S. Fracture initiation at sharp notches: correlation using critical stress intensities. Int J Solid Struct 1997;34:3873–83.
[9] Dunn ML, Suwito W, Cunningham S, May CW. Fracture initiation at sharp notches under mode I, mode II, and mild mixed mode loading. Int J Fracture 1997;84:367–81.
[10] Gómez FJ, Elices M. Fracture of components with V-shaped notches. Engng Fract Mech 2003;70:1913–27.
[11] Gómez FJ, Elices M. A fracture criterion for sharp V-notched samples. Int J Fracture 2003;123:163–75.
[12] Boukharouba T, Tamine T, Nui L, Chehimi C, Pluvinage G. The use of notch stress intensity factor as a fatigue crack initiation parameter. Engng Fract Mech 1995;52:503–12.
[13] Verreman Y, Nie B. Early development of fatigue cracking at manual fillet welds. Fatigue Fract Engng Mater Struct 1996;19:669–81.
[14] Lazzarin P, Tovo R. A notch intensity approach to the stress analysis of welds. Fatigue Fract Engng Mater Struct 1998;21:1089–104.
[15] Atzori B, Lazzarin P, Tovo R. From a local stress approach to fracture mechanics: a comprehensive evaluation of the fatigue strength of welded joints. Fatigue Fract Engng Mater Struct 1999;22:369–82.
[16] Lazzarin P, Livieri P. Notch stress intensity factors and fatigue strength of aluminium and steel welded joints. Int J Fatigue 2001;23:225–32.
[17] Reedy Jr ED. Asymptotic interface-corner solutions for butt tensile joints. Int J Solid Struct 1993;30:767–77.
[18] Reedy Jr ED, Guess TR. Comparison of butt tensile strength data with interface corner stress intensity factor prediction. Int J Solid Struct 1993;30:2929–36.
[19] Aliabadi MH, Rooke DP. Numerical fracture mechanics. Dordrecht: Kluwer Academic Publishers; 1991.
[20] Anderson TL. Fracture mechanics, fundamental and application. New York: CRC press; 2005.
[21] Tada H, Paris CP, Irwin GR. The stress analysis of cracks handbook. 3rd ed. New York: ASME; 2000.
[22] Murakami Y. Stress intensity factors handbook, vols. 4–5. Berlin: Springer; 2001.
[23] Shin CS, Man KC, Wang CM. A practical method to estimate the stress concentration of notches. Int J Fatigue 1994;16:242–56.
[24] Livieri P. A new path independent integral applied to notched components under mode I loadings. Int J Fracture 2003;123:107–25.
[25] Zhao Z, Hahn HG. Determining the SIF of a V-notch from the results of a mixed-mode crack. Engng Fract Mech 1992;43:511–8.
[26] Chen DH. Stress intensity factors for V-notched strip under tension or in-plane bending. Int J Fracture 1995;70:81–97.
[27] Atzori B, Lazzarin P, Tovo R. Stress field parameters to predict the fatigue strength of notched components. J Strain Anal 1999;34:437–53.
[28] Strandberg M. A numerical study of the elastic stress field arising from sharp and blunt V-notches in a SENT-specimen. Int J Fracture 1999;100:329–42.
[29] Strandberg M. Upper bounds for the notch intensity factor for some geometries and their use in general interpolation formulae. Engng Fract Mech 2001;68:577–85.
[30] Noda N, Takase Y. Generalized stress intensity factors for V-shaped notch in a round bar under torsion, tension and bending. Engng Fract Mech 2003;70:1447–66.
[31] Xu RX, Thompson JC, Topper TH. Practical stress expressions for stress concentration regions. Fatigue Fract Engng Mater Struct 1995;18:885–95.
[32] Irwin GR. Fracture. Handbuch der physik, vol. 6. Berlin: Springer; 1958. p. 551–90.
[33] Creager M, Paris PC. Elastic field equations for blunt cracks with reference to stress corrosion cracking. Int J Fract Mech 1967;3:247–52.
[34] Glinka G. Calculation of inelastic notch-tip strain-stress histories under cyclic loading. Engng Fract Mech 1985;22:839–54.
[35] Hasebe N, Kutanda Y. Calculation of stress intensity factors from stress concentration factor. Engng Fract Mech 1978;10:215–21.
[36] Lazzarin P, Tovo R. A unified approach to the evaluation of linear elastic stress fields in the neighborhood of cracks and notches. Int J Fracture 1996;78:3–19.
[37] Filippi S, Lazzarin P, Tovo R. Developments of some explicit formulas useful to describe elastic stress fields ahead of notches in plates. Int J Solid Struct 2002;39:4543–65.
[38] Lazzarin P, Filippi S. A generalised stress intensity factor to be applied to rounded V-shaped notches. Int J Solid Struct 2006;43:2461–78.
[39] Lazzarin P, Zappalorto M, Yates JR. Analytical study of stress distributions due to semi-elliptic notches in shafts under torsion loading. Int J Engng Sci 2007;45:308–28.
[40] Zappalorto M, Lazzarin P, Yates JR. Elastic stress distributions resulting from hyperbolic and parabolic notches in round shafts under torsion and uniform antiplane shear loadings. Int J Solid Struct 2008;45:4879–901.
[41] Inglis CE. Stresses in a plate due to the presence of cracks and sharp corners. Trans Inst Naval Arch 1913;55:219–30.
[42] Neuber H. Theory of notch stresses. 2nd ed. Berlin: Splinger-Verlag; 1958.
[43] Benthem JP, Koiter WT. In: Sih GC, editor. Mechanics of fracture 1. Noordhoff Int Pub 1; 1973. p. 131–78.
[44] Lazzarin P, Sonsino CM, Zambardi R. A notch stress intensity approach to predict the fatigue behaviour of T butt welds between tube and flange when subjected to in-phase bending and torsion loading. Fract Engng Mater Struct 2004;27:127–41.
[45] Chen Jt, Chen KH, Yeih W, Shieh NC. Dual boundary element anaysis for cracked bars under torsion. Engng Computation 1998;15:732–49.